

# Characterisation of MEMs mirrors for use in atmospheric and ocular wavefront correction

Nicholas Devaney, Derek Coburn, Chris Coleman, J.Christopher Dainty, Eugenie Dalimier, Thomas Farrell, David Lara, David Mackey, Ruth Mackey  
Applied Optics Group, Department of Experimental Physics, National University of Ireland,  
Galway, Ireland

## ABSTRACT

The Applied Optics group at the National University of Ireland, Galway, is engaged in research into various aspects of the application of adaptive optics to both ocular and atmospheric wavefront correction. A large number of commercially available deformable mirrors have been selected by the group for AO experiments, and these mirrors have been carefully characterised to determine their suitability for these tasks. In this paper we describe the approach we have used in characterising deformable mirrors and present results for several MEMs mirrors, including membrane mirrors from AgilOptics and Flexible Optical BV, a segmented micromirror from IrisAO and a 140-actuator mirror from Boston micromachines.

**Keywords:** Adaptive Optics, Deformable mirrors, Wavefront correctors

## 1. INTRODUCTION

Deformable mirrors are the usual form of wavefront corrector used in adaptive optics (AO) systems. Many types are available to the AO designer. The mirror faceplate may be continuous or segmented, and while most deformable mirrors are continuous, we also present here the results of tests on a segmented mirror, a 37-segment mirror from IrisAO. The deformable mirror actuation may be based on position or force. Position actuators include piezoelectric and electrostrictive actuators. Force actuation usually employs electrostatic or magnetic fields, and we present the results of tests on mirrors using both types of actuation.

The suitability of a deformable mirror to a particular task depends on that task, and so a mirror which is suitable for correcting aberrations in one situation may not be suitable for a different use. Adaptive optics was originally developed for the correction of aberrations due to atmospheric turbulence. The applications include recovering diffraction-limited spatial resolution in ground-based telescopes<sup>1</sup>, and pre-correcting laser beams for optical communications. More recently, adaptive optics has been used to correct ocular aberrations, allowing diffraction-limited imaging of the retina<sup>2</sup>. The possibility of using adaptive optics to provide 'super-vision' has also been investigated<sup>3</sup>. The Applied Optics group at NUI, Galway has acquired several deformable mirrors for use in projects in the areas of adaptive correction of both atmospheric turbulence and ocular aberrations. We have already published some results of testing these mirrors<sup>4-6</sup>, and this paper presents additional results on some of those mirrors, as well as the results of testing some new mirrors.

This paper is organised as follows; in part 2 we present the mirrors which have been tested, with emphasis on the mirrors which we have not previously described. In part 3 we summarise the technique used to analyse the performance of the mirrors for the specific tasks of correcting ocular and turbulent atmospheric aberrations, and in part 4 we present comparative results. It should be noted that we will not examine the dynamic performance of these mirrors in this work.

## 2. MIRRORS TESTED

The mirrors we have studied are:

- a 37-channel micromachined membrane deformable mirror (MMDM) from Flexible Optical BV (OKO37)
- a 37-channel MMDM from AgilOptics (AgilOptic37)
- a 37 channel segmented deformable mirror from Iris AO (IrisAO37)

- a 19-channel piezoelectric mirror from Flexible Optical BV (OKO19\_PZT)
- a 37-channel piezoelectric mirror from Flexible Optical BV (OKO37\_PZT)
- a 35-channel bimorph deformable mirror from AOptix (AOptix35)
- a 52-channel magnetic deformable mirror from Imagine Eyes (MIRAO52)
- a 140-channel MEMS device from Boston Micromachines (BMC140).

The characteristics of these mirrors are reported in Table1, and their actuator layouts are shown in Figure 1.

Table 1. Characteristics of the mirrors tested.

Mirror	Technology	Diameter (mm)	Actuators	Individual stroke ( $\mu\text{m}$ )	Total stroke ( $\mu\text{m}$ )
OKO37	Electrostatic	15	37	0.3-0.6	3.5
OKO19_PZT	Piezoelectric	30	19	3, 7-9	--
AOptix35	Bimorph	10.2	35	3, 7	16
MIRAO52	Magnetic	15	52	10-15	25
BMC140	Electrostatic	3.3×3.3	140	1.5	3.5
AgilOptics37	Electrostatic	16	37	0.2-0.6	4.5
IrisAO37	Electrostatic	3.5	37	5	--
OKO37_PZT	Piezoelectric	30	37	2, 3.5-5	--

Note: The total stroke is the peak-to-valley of the surface deformation when the maximum command voltage is applied to all actuators. The values for the MIRAO52 are for half its full range, as the manufacturers recommend not to operate it continuously beyond this. The OKO37 and AgilOptics37 individual stroke values are for edge and central actuators.

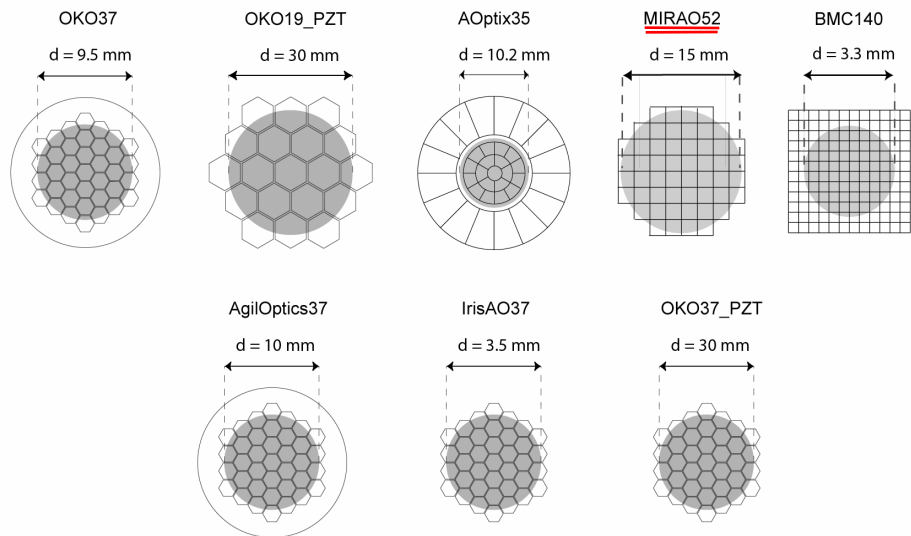


Figure 1 Actuator layout of the mirrors tested, with the typical optical pupil superimposed.

The mirrors for which we have not previously published results are the AgilOptics37, the IrisAO37 and the OKO37\_PZT. The AgilOptics device detailed in the current study is a 16mm diameter 37 electrode membrane device with a hexagonal electrode packing as illustrated in Figure 1. The mirror, the Multi37, is based on a micromachined silicon-nitride membrane and has similar dimensions and electrode geometry to that of the OKO37 membrane mirror. This device is one of a set of multielectrode membrane mirrors manufactured by AgilOptics, a group of which have been made available to the Applied Optics Group in NUI, Galway for testing and evaluation. A key feature of the range of AgilOptics mirrors is the snap down protection whereby the device can snapdown without damaging the mirror membrane, allowing snapdown voltage and the corresponding maximum stroke of the device to be assessed (snapdown is often fatal in other membrane mirrors).

In the tests reported here we drove the electrodes to a maximum of 245V as recommended by the manufacturer. The stroke obtained with these measurements are in keeping with the advertised operating range detailed for this family of mirrors (as is the surface flatness of 360nm PTV / 64nm rms). It should be noted however that in tests the mirror could be pushed to greater than 280 V before snapdown was observed. This adds significantly to the stroke achievable with the mirror with the stroke scaling as the square of the electrode voltage; a factor which should be taken into account in making mirror comparisons. As with the OKO membrane study (the second of the membrane mirrors detailed here), the optical pupil used in aberration correction was reduced to  $\sim 2/3$  of the membrane diameter ( $\sim 10$  mm). This  $2/3$  reduction is a commonly accepted figure adopted to facilitate correction of aberrations at the edge of the pupil addressing the fact that the membrane is clamped to the edge. The OKO19\_PZT and OKO37\_PZT have free edges, and hence the sum of all the influence functions does not produce wavefront deformation.

The IrisAO37 consists of 37 hexagonal, single-crystal silicon mirror segments, each measuring 700 microns vertex to vertex. The gaps between the segments are less than 5 microns and the total usable inscribed aperture has a diameter of 3.5mm. Each segment is supported by bimorph flexures and incorporates three electrostatic actuators, allowing piston, tip and tilt actuation. The mirror comes with a pre-calibrated driver, allowing open-loop control. While the segments are independent of one another, the control of the mirror is complicated by coupling between the actuators of the individual segments.

### 3. PERFORMANCE ANALYSIS METHOD

The performance of the mirrors has been determined by fitting to wavefronts simulated to have aberrations with statistics corresponding to either a Kolmogorov model of atmospheric turbulence or the Thibos model of ocular aberrations<sup>7</sup>. The fitting performance requires determining the mirror modes, and these were determined from laboratory measurements of the actuator influence functions. The measurements for all mirrors except the segmented mirror were obtained using a FISBA interferometer, which is a commercial Twyman-Green system. Each measured influence function, which corresponds to the phase measured when a single actuator is poked, forms a column of the mirror's interaction matrix,  $M$ . A singular value decomposition of  $M$  gives  $M=UWV^T$ , and the columns of  $U$  form an orthonormal basis for the mirror. The  $W$  matrix is diagonal, and the diagonal elements are the singular values. The inverse of these values give a measure of how much stroke is required to produce the corresponding mode. An equivalent analysis consists of finding the eigenvectors of  $MM^T$ , which is referred to as the actuator cross-coupling matrix. When the modes of the mirror are known, the best fit mirror shape corresponding to a given aberrated wavefront,  $\phi$ , is given by the projection

$$a = U^T \phi$$

where  $a$  is a vector of mirror mode coefficients. The corresponding vector of actuator commands,  $c$ , is given by

$$c = VWU^T \phi$$

while the mirror shape is given by

$$\hat{\phi} = UU^T \phi$$

The residual wavefront error is given by  $\hat{\phi} - \phi$ . However, this does not take into account the limited stroke of the mirror. Small singular values can cause the mirror to saturate, and so the singular values which are relatively small are

set to zero if necessary. In addition, a clipping function is applied to the command voltages and then projected onto the mirror mode command basis in order to find the new combination of mirror modes

$$\hat{\phi}_{clipped} = U W V^T f(c_\phi)$$

where

$$f(c_\phi) = \begin{cases} c_i & \text{if } |c_i| \leq c_{lim} \\ c_{lim} \times \frac{c_i}{|c_i|} & \text{if } |c_i| > c_{lim} \end{cases}$$

In some cases we also checked the ability of the mirrors to generate individual Zernike modes. Figure 2 shows rms values of the maximum Zernike before the onset of clipping for the OKO37 membrane mirror. The rms residual wavefront errors predicted according to the analysis presented above, and actually measured with the FISBA interferometer, are also presented. The difference between the measured and predicted residuals are all less than 15nm rms. This corresponds to an upper limit for the non-linearity of this mirror, which has been the subject of recent study<sup>9</sup>.

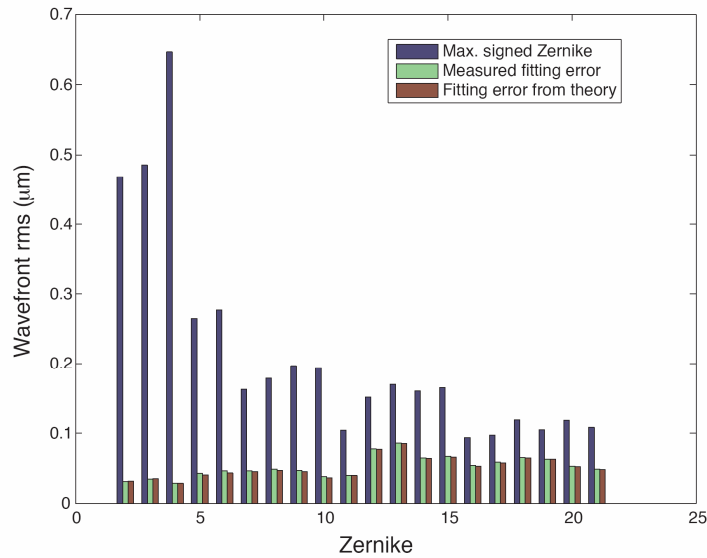


Figure 2 The maximum signed Zernike the OKO37 can produce and the corresponding fitting error from measured wavefronts and from simulation of modal fitting

Figure 3 and Figure 4 show the results of a similar analysis for the IrisAO37 segmented mirror. In the case of this mirror, the surface measurements have been made using a Zygo New View white light interferometer. For each Zernike polynomial, the least squares best fit piston, tip and tilt is calculated for each segment. Part of the difference between the predicted and measured residuals shown in Figure 4 are due to errors in the Smartdriver used to position the segments in open loop. This should position the segments to better than 30nm rms, but has not been calibrated for some time. Another part of the difference will be due to figure errors of the individual segments.

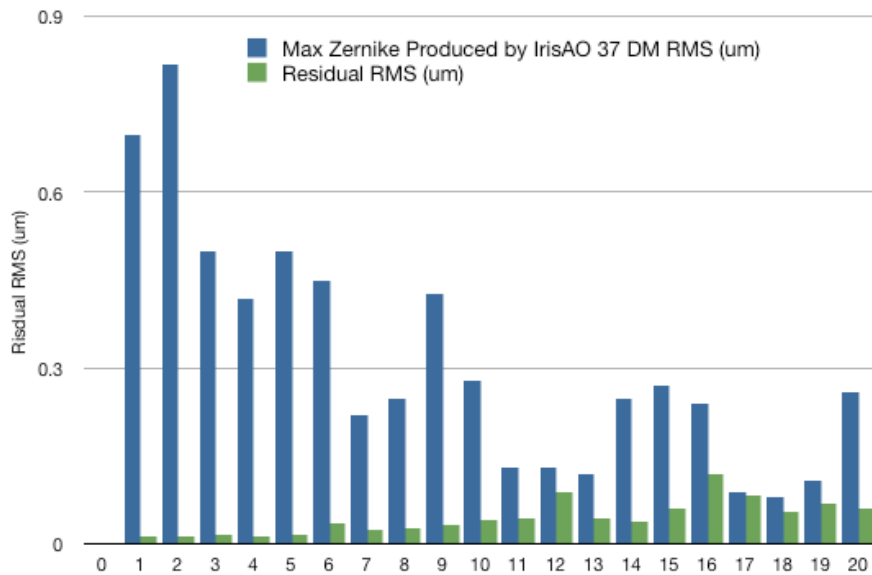


Figure 3 The maximum signed Zernike the IrisAO segmented mirror can produce and the corresponding fitting error from simulation of modal fitting

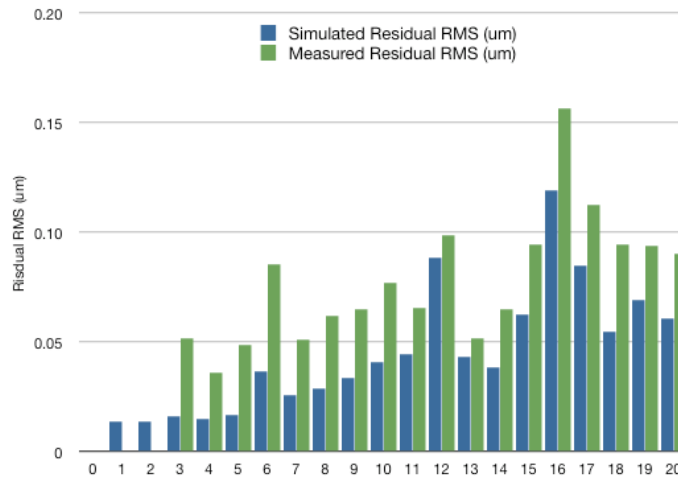


Figure 4 Comparison of simulated and measured residuals obtained with the IrisAO segmented mirror when producing individual Zernike polynomials.

## 4. PERFORMANCE RESULTS

### 4.1 Performance for the correction of ocular aberrations

Correcting ocular wavefront aberrations is one of the main current applications of adaptive optics techniques. In previous papers<sup>3-5</sup>, we simulated the performance of five different deformable mirrors in correcting ocular aberrations. We used the least-square methodology described in Section 3, and 6 mm diameter ocular wavefronts generated using a model<sup>7</sup> derived by Thibos *et al.* from a large sample ocular wavefront data set<sup>8</sup>. We calculated the best fit that could be obtained

from each mirror for 100 simulated ocular wavefronts. The ocular wavefronts had a mean wavefront error rms of 0.68  $\mu\text{m}$ . The results are given in terms of residual wavefront error rms, averaged over the 100 wavefronts and given for the optimized number of modes for each mirror. Due to limited stroke, some mirrors exhibit saturation when applying the least-square fitting method, and a better correction is achieved with a limited number of modes<sup>3</sup>. The data are presented in Figure 5, along with reported data from the previous five mirrors tested. Concerning the previous data, the figures given here are slightly smaller than those given previously, due to some measurement artifacts that have since been removed. This affects in particular the MIRA052 mirror performance: the given best mean wavefront error rms is here 0.017  $\mu\text{m}$ , as compared to the value of 0.06  $\mu\text{m}$  given in a previous paper<sup>6</sup>.

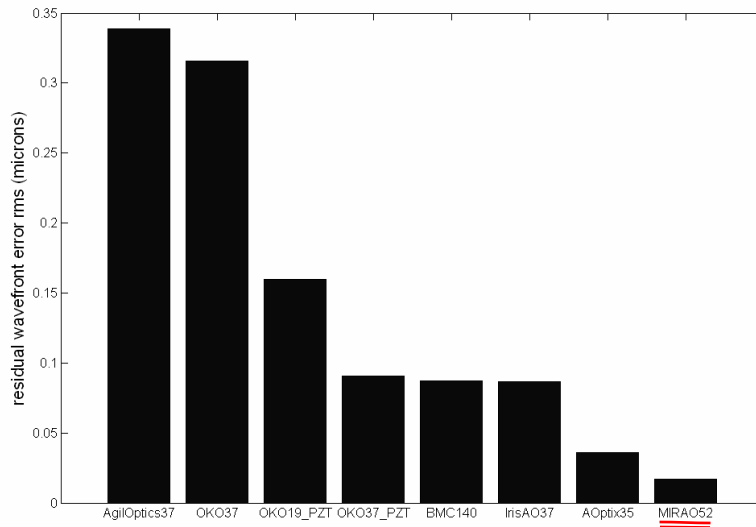


Figure 5 Mean residual wavefront error rms averaged over 100 ocular wavefronts after the best fit given by the mirrors.

Figure 5 gives a ranking of the mirrors for the correction of ocular aberrations. It appears that one cannot predict the performance of a particular mirror in correcting ocular aberrations from its stroke or number of actuators alone. Very different mirrors have similar performance (such as the OKO37\_PZT, the BMC140 and the IrisAO37) while mirrors with similar stroke and number of actuators (such as the OKO37\_PZT and the AOptix35) can exhibit very different performance. Figure 6 shows an example of the residuals for ocular wavefront correction by the different deformable mirrors; one can appreciate the very different patterns of wavefront errors produced by the mirrors.

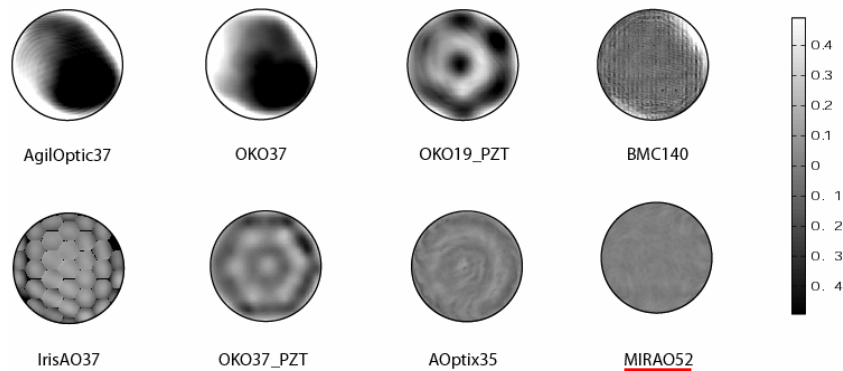


Figure 6 Wavefront residuals after fitting of a typical ocular wavefront with the deformable mirrors (scale in microns).

More insight into the limitations of the mirrors for this particular task can be gained from a spatial frequency analysis of the residual wavefront maps after simulated correction. For most of the mirrors we calculated the radial average of the Fourier spectrum of each simulated ocular wavefront error residual, and averaged this profile over the 100 wavefronts; the results are presented in Figure 7. The calculations were not performed for the IrisAO37 mirror which is segmented and hence cannot be directly compared to the continuous mirrors in terms of spatial frequency content.

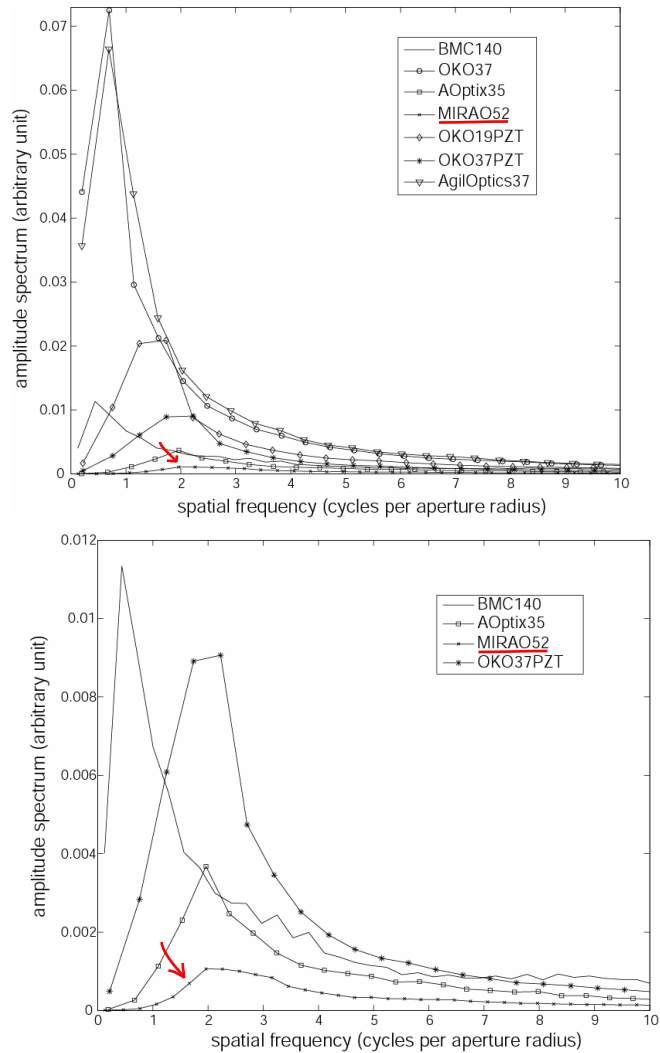


Figure 7 Radial amplitude spectrum of the wavefront error residual averaged over the 100 wavefronts (above), and a zoom on the best four mirrors curves (below).

From these figures we can make some points. As mentioned previously, the OKO37 has limited stroke, and hence it saturates for most eyes when applying the least-squares fit. The best fit is obtained for a limited number of modes (14), and the mean residual for 100 ocular wavefronts remains high. This saturation is visible in the wavefront map of Figure 6 and highlighted by the low frequency peak of the Fourier spectrum in Figure 7. The AgilOptics37, which shares many characteristics of the OKO37, unsurprisingly gives very similar simulation results. The stroke is not an issue for the OKO19\_PZT, but the residual wavefront plots as well as the corresponding spectrum in Figure 7 indicate that its performance is limited by the number and arrangement of actuators. A similar analysis can be made on the OKO37\_PZT. It is interesting to note that although the number and stroke of the actuators is similar for both the OKO37\_PZT and the

AOptix35, the former does not perform as well as the latter. Their wavefront residual maps in Figure 6 seem to reflect the actuator layout, and this is confirmed by their Fourier spectra. It can be inferred that the actuator layout here is critical. The AOptix35 outer ring of actuators, completely separated from the optical pupil, provides an arrangement well fitted to the ocular wavefronts, which are generally quite steep at the edge. The influence functions of these actuators produce slopes, rather than curvature deformations. In contrast, the OKO37\_PZT last ring of actuators is partially covered by the optical pupil and therefore cannot provide the necessary deformation. In particular, some influence functions are just centered on the outline of the pupil and will produce minimal wavefront slope on this outline. From the elements observed so far, it is not surprising that, although they have very different characteristics, the three mirrors BMC140, IrisAO37 and OKO37\_PZT, give similar mean residual wavefront error rms. As for the BMC140, the main limitation is the stroke, which again, is highlighted in the wavefront map in Figure 6 and the low frequency peak in Figure 7. The MIRA052 appears to be the best mirror for the correction of ocular aberrations. It exhibits enough stroke and a good layout of actuators; the spectrum of the residual wavefronts is much flatter than the others, and probably essentially reflects noise.

Finally, when discussing the fitting performance of the deformable mirrors, it may be relevant to take into account the initial deformation of the mirror, as this may further limit the available stroke of the mirror in correcting wavefronts. The initial shape of the mirror can be measured by interferometry at the command mid-range (for electrostatic devices) and tip, tilt and defocus should be removed, as these aberrations would easily be independently corrected in an adaptive optics system. The resulting wavefront error can then be added to the ocular wavefronts to be fitted in the simulations. Such calculations have shown that the bias has a very small effect on the MIRA052 (the mean residual wavefront error rms increased to 0.027 microns) However, the effect can be more important for other mirrors which have less stroke.

#### 4.2 Performance of the deformable mirrors for the correction of atmospheric aberrations

The spatial resolution of large ground-based telescopes is limited by the earth's turbulent atmosphere and adaptive optics is required to correct for these aberrations. It is interesting to compare the performance of our sample of deformable mirrors when correcting atmospheric turbulence and ocular aberrations. Correcting for the turbulent atmosphere typically requires a high bandwidth DM with stroke and actuator requirements defined by the ratio of pupil diameter,  $D$  to Fried's parameter,  $r_0$ , which is the coherence length of wavefronts after passing through the turbulence.

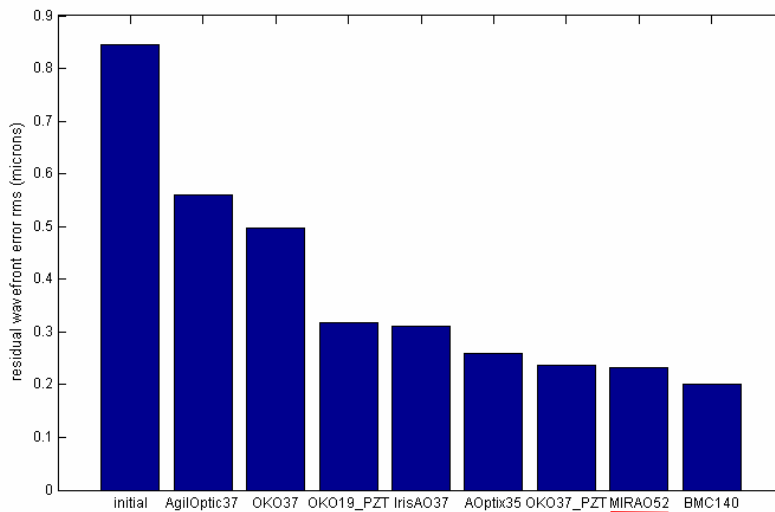


Figure 8 Mean residual rms wavefront error averaged over 100 phase screens obeying Komolgorov statistics with strength of  $D/r_0=9$ , but with piston, tip and tilt removed.

As in a previous study, the average residual rms error is calculated from an average of 100 Komolgorov phase screens using a least squares approach<sup>6</sup>. These screens have a power of  $D/r_0=9$  which corresponds to 0.84 micron rms wavefront

error at a wavelength of  $2.2\mu\text{m}$  after piston, tip and tilt are removed. Figure 8 shows the residual rms error for each mirror with the number of mirror modes used optimised for maximum correction. **Insufficient stroke is a limiting factor for nearly all the mirrors, except for the MIRA052 magnetic mirror.** The new mirrors to this comparison have very different performances with the AgilOptics37 suffering from actuator saturation. This would not be the case if a smaller value of  $D/r_0$  had been examined. The segmented IrisAO mirror performed better than the OKO37 but worse than the OKO37\_PZT, with all having the same number actuators. Indeed the relatively low cost piezoelectric OKO mirror shows excellent performance due to its well defined, linear influence functions and its large amount of available stroke. The residual wavefront maps for both 37 actuator OKO mirrors are given in Figure 9. The piezoelectric mirror does however have a large initial aberration, which reduces its dynamic range somewhat in closed loop adaptive optics and this isn't taken into account in this study.

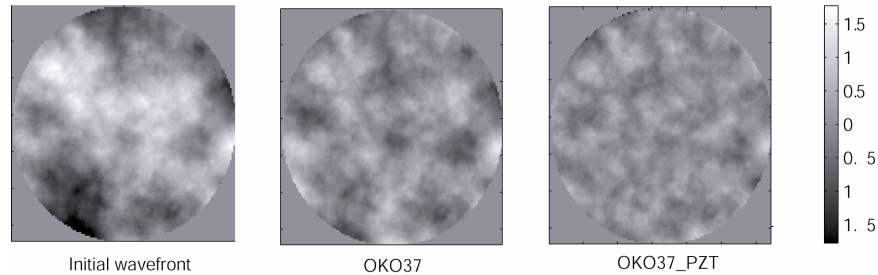


Figure 9 Residual wavefront maps after correction for a single Kolmogorov phase screen with rms error of 0.65 microns

## CONCLUSION

We have compared eight different deformable mirrors for the tasks of correcting both ocular and atmospherically aberrated wavefronts. The mirrors are all commercially available and cover a range of actuator types and geometries. The study was based on least-squares fitting using mirror modes derived from interferometrically measured influence functions. The mirrors were fitted to simulated wavefronts having statistics which are either Kolmogorov or following the Thibos eye model. It turns out that the relative performance cannot be predicted purely on the number of actuators and stroke. The actuator layout, and in particular the correction at the pupil edge is also seen to be important, especially in the case of correcting ocular wavefronts. The worst performance in correcting both ocular and atmospheric wavefronts is obtained with the membrane mirrors, and this is due to their limited stroke. However, it appears that the AgilOptics mirror could be driven with higher voltages than was recommended by the manufacturer before snapdown occurs, and this would significantly increase the stroke. **In the case of correcting ocular aberrations, the best performance was obtained with the MIRA052 magnetic mirror, and very good performance was also obtained with the Aoptix35 bimorph mirror.** The best performance in the case of correcting atmospheric wavefronts was obtained with the BMC140 micromirror, and again, **very good performance was obtained with the MIRA052 magnetic mirror.** Good performance was achieved in both cases with the 37-actuator piezoelectric mirror from OKO and the 37-element segmented mirror from IrisAO.

## ACKNOWLEDGEMENTS

We would like to thank the manufacturers of the deformable mirrors used in this study for their assistance. In particular we would like to thank AgilOptics who make available the evaluation mirror used in this study and their technical team for support provided. This research is funded by Science Foundation Ireland under Grant No. SFI/07/IN.1/1906.

## REFERENCES

- <sup>1</sup> N. Devaney, "Review of Astronomical Adaptive Optics systems and plans", Proc. SPIE 6584, 658407, (2007)
- <sup>2</sup> H. Hofer, L. Chen, G.Y. Yoon, B. Singer, Y. Yamauchi, D.R. Williams, "Improvement in retinal image quality with dynamic correction of the eye's aberrations", Optics Express, 8, 631-643 (2001)
- <sup>3</sup> E. Dalimier, C. Dainty and J.L. Barbur, "Effects of higher order aberrations on contrast acuity as a function of light level", Journal of Modern Optics, in press
- <sup>4</sup> E. Dalimier and C. Dainty, "Comparative analysis of deformable mirrors for adaptive optics in the eye", Opt. Express **13**(11), 4275-4285 (2005).
- <sup>5</sup> E. Daly, E. Dalimier, and C. Dainty, "Requirements for MEMS mirrors for adaptive optics in the eye", Proc. SPIE **6113**, 611309 (2006).
- <sup>6</sup> T. Farrell, E. Daly, E. Dalimier and C. Dainty, "Task-based assessment of deformable mirrors", Proc. SPIE **6467**, 64670F (2007).
- <sup>7</sup> L. N. Thibos, A. Bradley and X. Hong, "A statistical model of the aberration structure of normal, well-corrected eyes", Ophthal. Physiol. Opt. **22**(5), 427-433 (2002).
- <sup>8</sup> L. N. Thibos, X. Hong, A. Bradley and X. Cheng, "Statistical variation of aberration structure and image quality in a normal population of healthy eyes", J. Opt. Soc. Am. A **19**(12), 2329-2348 (2002).
- <sup>9</sup> E. Gendron, F. Vidal, F. Zamkotsian, T. Heurtebize, Z. Hubert, D. Perret, F. Chelma, P. Jagourel, "Experimental results on the open-loop control of an electrostatic DM for MOAO", in "Adaptive Optics: Analysis and Methods; Computational Optical Sensing and Imaging; Digital Holography and Three-Dimensional Imaging; and Signal Recovery and Synthesis on CD-ROM (The Optical Society of America, Washington, DC2007), ATuD2